RSC Advances

ROYAL SOCIETY OF CHEMISTRY

www.rsc.org/advances

Charge-transfer metal-organic frameworks based on CuCN architecture units: crystal structures, luminescence properties and theoretical investigations

Rong-Yi Huang,*[a] Chen Xue,[a] Chang-Hai Zhu,[a] Zhu-Qing Wang,[a] Heng Xu[a] and Xiao-Ming Ren*[b]

[a] *Anhui Key Laboratory of Functional Coordination Compounds, School of Chemistry and Chemical Engineering, Anqing Normal University, Anqing 246003, P. R. China*

[b] *Department of Applied Chemistry, Science College, Nanjing University of Technology, Nanjing, 210009, P. R. China*

Corresponding Author:

Rong-Yi Huang

Mailing Address: School of Chemistry and Chemical Engineering, Anqing Normal University, Anqing 246011, P. R. China

Telephone: +86-556-5500090

Fax: +86-556-5500090

E-mail: huangry@aqtc.edu.cn

Xiao-Ming Ren

Mailing Address: Department of Applied Chemistry, Science College, Nanjing University of Technology, Nanjing, 210009, P. R. China

E-mail: xmren@njut.edu.cn

ABSTRACT

Four CuCN complexes, namely $Cu_4(CN)_4(bix)_2$ (**1**), $Cu_2(CN)_2(bmimb)$ (**2**), $Cu_2(CN)_2(bmimb)$ (**3**) and $Cu_3(CN)_3(bimb)$ (**4**), have been prepared *via* the synchronous redox and self-assembly reaction of $Cu(NO_3)_2$, $K_4[Fe(CN)_6]$ and three structurally related flexible bis(imidazole) ligands 1,4-bis(imidazol-1-ylmethyl) benzene (bix), 1,4-bis(2-methylimidazol-1-lmethyl)benzene (bmimb) and 4,4`-bis(1-imidazolyl-1-ylmethyl)biphenyl (bimb) under solvothermal conditions. Although all prepared complexes contain one-dimensional CuCN subchains, they have different structures of 2_1 helical chain, *meso*-helical chain, 2_1-helical chain and zigzag chain for **1**, **2**, **3** and **4**, respectively. Complex **1** presents a three-dimentional framework with (10, 3)-d (utp) topology and exhibits an interesting five-fold interpenetration structures attributed class Ia type. Moreover, the five-fold entangled network is turned into an unprecedented three-dimentional binodal (3,6)-connected self-penetrated network *via* the Cu···Cu bond interactions. Most interestingly, **2** and **3** are a pair of isomers, and also generate a three-dimentional uninodal (10, 3) network with $ThSi_2$ and utq topology, respectively, which all display an interesting three-fold interpenetration, and also belong to Class Ia type. Complex **4** displays a distorted two-dimentional (6, 3) topology layer, and further forms a three-dimentional supramolecular structure by weak $\pi\cdots\pi$ interactions. It is indicated that the organic ligands play a crucial role in the final product structures as well as the solvents. Meanwhile, the complexes present strong green (λ_{max} = 553(**1**), 565(**2**), 565(**3**) and 563 nm (**4**)) photoluminescence as power in the solid state at room temperature. The theoretical calculations show that the intense green experimental band can be assigned to a combination of the cyanide group to copper(I) center and cyanide group to cyanide group charge transfer transitions. Additionally, the thermal analyses show that complexes **1-4** possess high thermal stabilities.

Keywords: Cuprous cyanide; Bis(imidazole) ligand; Crystal structure; Luminescence; Quantum chemical calculation

1. Introduction

Recently, the rational design and assembly of coordination polymers is ongoing area of research not only because of their intriguing architectures and topologies,[1] but also for their potential uses used as solid-state functional crystalline materials in the areas of catalysis, absorption, molecular recognition, ion exchange, magnetism, optics, and so on.[2] Particularly, among the family of coordination complexes, the luminescent coordination complexes containing heavy metal cores have also been wildly investigated,[3] and they present diverse architectures and effective applications in the area of organic light-emitting diode (OLED).[4] To date, the luminescent coordination complexes involving iridium, platinum, gold and ruthenium for this practical application have been the most extensively exhibited.[4] Moreover, the more available substitution of these noble metals has attracted remarkable interest and was also a significant challenging task because of their toxicity, their prices and their limited availability. In this process, the cuprous complexes appear to be an excellent candidate.[5] Additionally, it is well known that the inherent natures of the organic bridging ligands, such as coordination modes, coordination capability, configuration, substituent and flexibility/rigidity play a crucial role in generating the resulting architectures of coordination networks,[6] and the geometrical structures of organic bridging ligands can be expediently modified *via* organic synthesis. Although the crystal engineers have always attempted their best to explore the correlation between the organic bridging ligands and the resulting architectures and properties, it remains a long-term challenging task due on many factors affecting the assembly process of coordination polymers.[7] Currently, the neutral imidazole-containing bridging organic ligands as assembly blocks have attracted significant interest for their excellent coordination capacities, and potential applications in advanced materials.[8] Up to now, many fantastic coordination architectures based on the flexible/rigid imidazole-containing ligands have been generated, but the investigation of flexible/rigid imidazole-containing CuCN complexes is still less developed.[9]

Therefore, much more systematic work should be done in this topic. In our previous work, many intriguing coordination frameworks have been deeply investigated based on the appropriate flexible/rigid N-containing organic ligands.[10] As the continuation of our previous studies, we are focused on exploring the effect of the nature of flexible bis(imidazole) bridging ligands 1, 4-bis(imidazol-1-ylmethyl)benzene (bix), 1, 4-bis(2-methylimidazol-1-ylmethyl)benzene (bmimb) and 4, 4`-bis(1-imidazolyl-1-lmethyl)biphenyl (bimb) and solvents on the formation of their CuCN coordination frameworks in the present work. As a result, four CuCN complexes with different topology architectures, $Cu_4(CN)_4(bix)_2$ (**1**), $Cu_2(CN)_2(bmimb)$ (**2**), $Cu_2(CN)_2(bmimb)$ (**3**) and $Cu_3(CN)_3(bimb)$ (**4**) have been successfully obtained *via* a coincidental redox and self-assembly reaction of Cu(II) used as commencing materials under the solvothermal conditions, and have good thermal stabilities and green photoluminescent properties.

2. Experimental and computational sections

2.1. Materials and general methods

Three flexible bis(imidazole) ligands bix, bmimb and bimb were synthesized according to the reported procedures.[11] All other commercially available chemicals and solvents of A. R. grade employed were used without further purification. Elemental analyses for C, H and N were determined on an Elementar Vario EL III elemental analyzer. Infrared spectra were recorded on an AVATAR-360 (Nicolet Company) FT-IR spectra-photometer in the range of 4000–400 cm^{-1} with KBr pellets. The solid-state emission spectra were obtained on a Hitachi F-4500 fluorescence spectrophotometer at ambient temperature. Thermo gravimetric analyses (TGA) were carried out on a Netzsch STA-409PC thermoanalyzer in flowing N_2 (25-800 ^oC)at a heating rate of 10 ºC min^{-1}.

*2.2. Synthesis of complexes **1-4***

$Cu_4(CN)_4(bix)_2$ (1) A mixture containing $Cu(NO_3)_2 \cdot 3H_2O$ (48.3 mg, 0.2 mmol), $K_4[Fe(CN)_6] \cdot 3H_2O$ (42.2 mg, 0.1 mmol), bix (23.8 mg, 0.1 mmol), CH_3OH (8 mL) and H_2O (8 mL) was heated at 160 ºC for 4 days in a 25 mL stainless steel autoclave with a Teflon liner and kept under autogenous pressure. After the autoclave was slowly cooled down to room temperature, yellow block crystals of **1** suitable for single crystal X–ray crystallographic analysis were collected by filtration and rinsed with distilled water and ethanol several times with a yield of 45% (based on Cu elemental). Anal. calcd for $C_{16}H_{14}N_6Cu_2$: C, 46.04; H, 3.38; N, 20.13. Found: C, 46.10; H, 3.32; N, 20.09%. IR (KBr pellet, cm^{-1}): 3118(m), 2926(w), 2858(w), 2106(s), 2085(s), 1642(m), 1514(s), 1438(m), 1388(w), 1351(w), 1281 (w), 1084(m), 933(w), 830(w), 754(m), 714(m), 655(m), 619(w), 473(w).

$Cu_2(CN)_2$(bmimb) (2) An identical procedure for preparing **2** was followed to prepare **1,** except bix was replaced with bmimb (26.6 mg, 0.1 mmol). Yellow rod crystals of **2** were obtained in 70% yield (based on Cu elemental). Anal. calcd for $C_9H_9N_3Cu$: C, 48.53; H, 4.07; N, 18.87. Found: C, 48.49; H, 4.09; N, 18.82%. IR (KBr pellet, cm^{-1}): 3121(w), 2924(w), 2854(w), 2123(s), 1594(w), 1533(m), 1507(m), 1473(m), 1441(m), 1415(s), 1338(w), 1284(m), 1151(m), 1135(m), 1074(w), 996(w), 755(s), 747(s), 671(m), 563(w).

$Cu_2(CN)_2$(bmimb) (3) The procedure for preparing **3** was similar to that described for preparing **2**, except that C_2H_5OH (8 mL) was replaced with CH_3OH (8 mL), and Yellow rod crystals of **3** were obtained. Yield: 75% (based on Cu elemental). Anal. calcd for $C_9H_9N_3Cu$: C, 48.53; H, 4.07; N, 18.87. Found: C, 48.55; H, 4.10; N, 18.81%. IR (KBr pellet, cm^{-1}): 3122(m), 2924(w), 2854(w), 2121(s), 1629(m), 1505(m), 1473(m), 1440(m), 1416(s), 1383(w), 1341(w), 1074(w), 1040(w), 996(w), 837(w), 747(s), 671(m), 561(m), 474(w), 435(w).

$Cu_3(CN)_3$(bimb) (4) An identical procedure for preparing 4 was followed to prepare 1, except bix was replaced with bimb (31.4 mg, 0.1 mmol). Yellow block crystals of complex 4 were obtained. Yield: 43% (based on Cu elemental). Anal. calcd for $C_{23}H_{18}N_7Cu_3$: C, 47.38; H, 3.11; N, 16.82. Found: C, 47.43; H, 3.07; N, 16.7%. IR (KBr pellet, cm^{-1}): 3127(m), 2936(w), 2845(w), 2114(s), 1636(m), 1523(m), 1448(s),

1380(w), 1342(w), 1308(w), 1102(m), 1023(w), 932(w), 843(w), 749(m), 722(w), 675(m), 625(m), 609(w), 567(w), 476(w), 459(w).

2.3. X-ray crystallography study

Crystal data collections and experimental detailes for **1**–**4** are presented in Table 1. All measurements were carried out on a Bruker Smart CCD area detector diffractometer with graphite-monochromated Mo-Kα radiation (λ = 0.71073 Å). The structures of complexes **1**-**4** were solved via direct method, and all non-hydrogen atoms were located from the trial structure and then refined anisotropically on F^2 by the full-matrix least-squares technique with the SHELXL-97 software package. The hydrogen atoms on carbon atoms were added geometrically and refined with a riding model. The bridged C/N atoms of the disorder cyanide anion in **2**–**4** are refined with the site occupancies 0.5C+0.5N and labled as X. All calculations were performed with the SHELXL-97 crystallographic software package.[12] The selected bond lengths and angles are listed in Table 2.

2.4. Computational details

To get better insight into the photoluminescence and electronic properties for **1**-**4**, The density function theory (DFT) and time-dependent DFT (TD-DFT) computations were performed on a minor calculational model selected from crystal structure measurements, and only the hydrogen positions were optimized. All computations were performed with the Gaussian09 D.01 software package[13] using the the hybrid Becke-Lee-Yang-Parr's functional B3LYP method.[14] The standard basis set 6-311++G(d, p)[15] for C, H and N, and LANL2DZ with an effective core potential (ECP)[16] for Cu(I) ion were used for all calculations. The computational results were visualized using GaussView 5.09 program.

3. Results and discussion

3.1. Synthesis and spectral characterization

The solvothermal synthesis was adopted in the present work. Complexes **1**–**4** containing CuCN architecture units were produced *via* a coincidental redox and self-assembly reaction of Cu(II) used as commencing materials. As is well known, under the solvothermal conditions, the Cu(II) ion can be expediently reduced by the $[Fe(CN)_6]^{4-}$ anion to form stable Cu(I) complex, and the produced cyanide anion was from decomposition of $K_4[Fe(CN)_6]\cdot 3H_2O$.[17] A reasonable mechanism under the solvothermal condition is illustrated in Scheme S1. Additionally, complexes **1**–**4** were all air stable, and could not dissolve in H_2O and common solvents. The elemental analyses indicate that the components of **1**–**4** were well in accordance with the results of the X-ray diffraction analysis. The infrared spectra corresponding to cyanide group stretching vibrations for the title complexes exhibit strong absorption bands in the 2111–2123 cm^{-1} range, which a characteristic bridging cyanide group stretching mode. All these are consistent with the results of crystal structural analyses.

3.2. Description of crystal structure

Structure of $Cu_4(CN)_4(bix)_2$ (1). Complex **1** crystallizes in monoclinic space group $P2_1/c$, its asymmetric unit consists of two independent copper(I) centers, two cyanide anions together with two types of bix ligands, which are all located on crystallographic inversion centers. As displayed in Fig. 1a, each copper(I) centre adopts a triangle coordinated geometry with two nitrogen atoms from one cyanide anion and one bix ligand, respectively, one carbon atom from another cyanide anion (Cu1 and Cu2 show different coordination environments). The Cu–N bond lengths fall in the range 1.912(2)–2.057(2) Å and the Cu–C bond lengths are 1.879(2) and 1.917(3) Å, and the angles of copper(I) center fall in the range 99.04(8)–143.72(10)° (ref. Table 2). The bond lengths and angles around Cu1 are somewhat different from those around Cu2. Moreover, the adjacent copper(I) centers are linked by the cyanide anion with μ_2 bridging fashion to form a one-dimensional (1-D) 2_1-helical chain running along the *b* axis with a pitch of 15.3787(8) Å (see Fig. 1b). The C–Cu–N angles in the 2_1–helical CuCN chains are 121.3(1)° (C–Cu1–N) and 143.7(1)°

(C–Cu2–N). The intrachain adjacent Cu···Cu distances are 4.9252(4) Å and 4.9196(5) Å, respectively. The adjacent 2_1-helical CuCN chains are further linked by the *anti*-bidentate bix ligands with two terminal nitrogen atoms distances of 11.1002(5) (Cu1-bix-Cu1) and 10.9918(3) (Cu2-bix-Cu2) Å, respectively, and form three-dimensional (3-D) framework containing two types of $[Cu_{10}(CN)_8(bix)_2]$ rings, which represents large quadrangle-shaped channels with the dimensions of approximately 12.64 Å × 14.24 Å in cross section along the *b* axis (Fig. S1). As described above, both Cu1 and Cu2 centers are considered to be 3-connected nodes, the cyanide and bix ligands can be simplified to linear linker from a topological perspective. TOPOS[18] analysis of the 3-D framework of **1** presents the (3, 3)-connected binodal network with the point symbol $(10^3)(10^3)$ topology[19], which belongs to (10, 3)-d (utp) network with the extended point symbol of $[10_2\cdot10_4\cdot10_4][10_2\cdot10_4\cdot10_4]$ (Fig. 1c). The single 3-D network of **1** contains large windows, so **1** adopts 5-fold interpenetration to minimize extremely large voids and stabilize the framework (Fig. 1d). Notably, owing to the 5-fold interpenetration, the whole structure has no residual void space in the whole crystal analyzed by PLATON program. Most interestingly, the whole interpenetration is obtained through pure translation. The translationally related five (10, 3)-d networks are observed showing the translational interpenetrating vector of [100] (8.79 Å), so **1** belongs to unusual Class Ia[20] interpenetration. Moreover, the smallest Cu1···Cu1 distances of the adjacent (10, 3)-d networks is 2.5664(1) Å, which presents a weak bond interaction between the two adjacent Cu1 centers, so the 5-fold interpenetration network is turned into a complicated 3-D framework. According to the topological view, such a complicated 3-D framework can be classified as an unprecedented binodal (3, 6)-connected network with the Point (Schläfli) symbol of $(6.8^2)_2(6^8.8^6.10)$ analyzed by TOPOS software package (Fig. 1e). Noticeably, in the binodal network, the Cu2 centers are simplified as 3-connected nodes (the Schläfli symbol is (6.8^2), the extended point symbol is $[6_2.8_5.8_7]$), and the $(Cu1)_2$ dimers can be simplified as 6-connected nodes (the Schläfli symbol is $(6^8.8^6.10)$, the extended point symbol is $[6.6.6.6.6.6.6.6.8_2.8_2.8_2.8_2.8_2.8_4.10_4]$. In addition, this network holds an intriguing

architecture of self-penetration, which was produced through the catenation occurring in one 6-membered circuit and one 10-membered circuit (Fig. 1e). To our knowledge, such a binodal (3, 6)-connected self-penetrated topological net has not been reported up to now.

Structure of $Cu_2(CN)_2$(bmimb) (2). Under the similar reaction conditions as in **1**, when the pendant substituent bis(imidazole) ligand bmimb was used instead of flexible ligand bix, a completely different framework of **2** was obtained. Complex **2** crystallizes in monoclinic space group *C*2/*c*. An asymmetric unit contains one unique copper(I) center, two types of cyanide anions (one locates on crystallographic inversion center, and another on the 2-fold axis) and half of one bmimb ligand located on crystallographic inversion center. As illustrated in Fig. 2a, copper(I) center is three-coordinated by two X atoms from two disordered cyanide anions, and one nitrogen atom from one bmimb ligand to produce a triangular geometry. The Cu–C/N bond lengths fall in the range 1.871(2)–2.0148(17) Å, and the angles of copper(I) center fall in the range 109.2(1)–129.3(1)° (Table 2). The site occupancy disordered cyanide anions also act as μ_2 bidentate bridging ligand, but each cyanide anion bridges two copper(I) centers to form a 1-D *meso*-helical infinite copper(I) cyanide chain running along the [101] direction with a pitch of 16.5169(8) Å (Fig. 2b). The X–Cu–X angles in the *meso*–helical CuCN chains are 129.3(1)°. The intrachain adjacent Cu···Cu distances are 4.9059(4) Å and 4.8969(5) Å, respectively. Then the adjacent *meso*-helical copper(I) cyanide chains are further jointed by the linear *anti*-bidentate bmimb ligand with two terminal nitrogen atoms distance of 10.5026(3) Å, and a 3-D framework was constructed consisting of large $[Cu_{10}(CN)_8(bmimb)_2]$ and $[Cu_{10}(CN)_6(bmimb)_4]$ rings. This 3-D framework contains larger open channels with the dimensions of approximately 10.48 Å × 24.48 Å in cross section along the [101] direction (Fig. S2). The copper(I) centers are also considered as 3-connected nodes, and the bmimb and cyanide anion ligands are both considered as the connectors from a topological point of view. As shown in Fig. 2c, each 3-connected node has three angles, and each of the angles forms a 10-membered shortest circuit, and hence the 3-D uninodal lattice has the well point symbol of 10^3.[19] The topological

analysis of **2** with TOPOS software further reveals that the 3-D uninodal network belongs to a (10, 3)-b ($ThSi_2$) network with the extended point symbol of $[10_2 \cdot 10_4 \cdot 10_4]$, which is completely different from the utp interpenetration observed in **1**. The single 3-D network consists of potential large channels, which are filled *via* mutual interpenetration of two independent equivalent networks, generating a 3-fold interpenetrated 3-D network (Fig. 2d). PLATON analysis indicates the whole structure still contains free void space of 232.9 Å, which occupies approximately 11.6% of the whole cell volume. In contrast to **1**, the methyl substituent of bmimb ligand should play a crucial role in making the interpenetration. Additionally, An analysis of the interpenetration shows that **2** also belongs to Class Ia according to the classification by Blatov and co-workers,[20] all the interpenetrated networks are generated only by translation, and the translating vector is [001] direction of 9.15 Å.

Structures of $Cu_2(CN)_2$(bmimb) (3) Interestingly, while keeping the similar bmimb ligand as in **2**, except that solvent methanol was replaced with ethanol, a new different isomer **3** was also presented. Complex **3** crystallizes in the orthorhombic *Fddd* space group (Table 1). The asymmetric unit of **3** also consists of one unique copper(I) center, half of one bmimb ligand located on crystallographic inversion center, and two kind of cyanide anions located on the *2*-fold axis. Similar to **1** and **2**, each copper(I) centre also adopts a triangle coordinated geometry with two X atoms from two different cyanide anions, respectively, and one nitrogen atom from one bmimb ligand, as displayed in Fig. 3a. The Cu–C/N bond lengths are in the range 1.887(3)–1.987(3) Å, and the angles of copper(I) center fall in the range 112.4(1)–123.6(1)° (Table 2). Moreover, the copper(I) centers are also linked by the cyanide anion with μ_2 bridging fashion to form a 1-D 2_1-helical chain running along the *a* axis with a pitch of 13.8683(25) Å (Fig. 3b). The X–Cu–X angles in the 2_1-helical CuCN chains are 123.60(2)°. The intrachain adjacent Cu···Cu distances are 4.8833(8) Å and 4.9515(7) Å, respectively. The adjacent 2_1-helical CuCN chains are also further linked by the *anti*-bidentate bmimb ligand with two terminal nitrogen atoms distance of 11.1217(7) Å, and form 3-D network consisting of large $[Cu_{10}(CN)_8(bmimb)_2]$ and $[Cu_{12}(CN)_8(bmimb)_4]$ rings. This 3-D framework is also

open, containing 1-D large channels of approximately 10.68 Å × 28.88 Å dimension in cross section along the crystallographic the *a* axis direction (Fig. S3). As described above, the copper(I) centers are also considered to be 3-connected nodes, the cyanide anion and bmimb ligands can also be simplified to linear linker from a topological perspective. TOPOS analysis of the 3-D network of **3** presents the 3-connected uninodal network with the point symbol 10^3 topology[19], which belongs to $3/10/t_2$ (utq) network with the extended point symbol of $[10\cdot10\cdot10_3]$ (Fig. 3c) which is completely different from the $ThSi_2$ interpenetration observed in **2** and the utp interpenetration observed in **1**. The single 3-D network of **3** also consists of large windows, so complex **3** adopts 3-fold interpenetration to minimize extremely large voids and stabilize the framework (Fig. 3d). The whole structure has still a total free void space of 336.4 $Å^3$ based on the PLATON calculations, which occupies 4.4% of the volume of the crystal cell. Moreover, the whole interpenetration is also produced through pure translations, and the translational vectors are [1/2 1/2 0] and [1/2 –1/2 0] directions of 13.42 Å, respectively. As described above, **3** also belongs to Class Ia[20] interpenetration. Complex **3** is the first utq topology network constructed based on the flexible bmimb ligand. The formation of **3** may be due to the nature of the solvent, which further shows the crucial effect of the solvent on the resulting structure.

Structure of $Cu_3(CN)_3$(bimb) (4). In a further explore, we employed a long flexible bis(imidazole) ligand bimb instead of flexible ligand bix with the similar reaction conditions as in **1**, and obtained a completely different network of **4**, which crystallizes in the triclinic space group *P*-1 and features a non–interpenetrated two-dimensional (2-D) coordination network. As shown in Fig. 4a, an asymmetric unit in **1** contains two independent copper(I) centers, two kind of cyanide anions, and half a bimb ligand. Each Cu1 center is three-coordinated with a triangular geometry, being coordinated by two cyanide anions (one disordered cyanide anion of them is located on a crystallographic inversion center) and one bimb ligand located on a crystallographic inversion center. The four atoms, Cu1, X1, C2 and N3, are approximately coplanar with a mean deviation of 0.0001 Å. The bond lengths and angles around the Cu1 center are in the range 1.867(7)–2.012(5) Å and

103.8(2)–134.7(2)° respectively, as listed in Table 2. The Cu2 center located on a crystallographic inversion center is two-coordinated by two cyanide anions via N atoms of the cyanide anions (Cu2–N2/N2A = 1.841(8) Å, N2–Cu2–N2A = 180.0°). The cyanide anion with μ_2 bridging fashion bridges adjacent copper(I) centers to form a one-dimensional zigzag chain running along the [110] direction (Fig. 4b). The Cu1–Cu1–Cu2 angle in the copper(I) cyanide chains is 134.3(3)°. The intrachain adjacent Cu1···Cu1/Cu2 distances are 4.9828(6) and 4.8564(5) Å, respectively. The adjacent copper(I) cyanide zigzag chains are further linked by the linear *anti*-bidentate bimb ligand with two terminal nitrogen atoms distance of 14.8589(20) Å, and form a distorted 2-D hexagonal grid sheet containing $[Cu_8(CN)_6(bimb)_2]$ rings with the dimensions of approximately 12.52 Å × 18.98 Å in the (–4 4 1) plane with a distorted (6, 3) net topology based on the 3-connected Cu1 center (Fig. 4c). Adjacent 2-D layers are further extended into a 3-D supramolecular structure through face to face π···π stacking interactions with centroid-to-centroid distance of 3.447(4)/4.207(4) Å between the two imidazole/benzene rings of adjacent bimb ligands (Fig. 4d). Interestingly, this supramolecular framework also contains a small 1-D channels of approximately 2.72 Å × 6.84 Å dimension in cross section running along the [110] direction (Fig. S4). PLATON calculations show that the free void space in the unit is about 14.3 $Å^3$, which occupies approximately 2.5 % of the whole cell volume.

3.3. Effect of assembly conditions on structures

The organic ligands play a crucial role in determining the molecular structures of the resulting complexes as well as the solvents. In this work, the structural characteristics of organic ligands such as substituent and size are the fundamental factor for structural difference with this series of CuCN complexes. To explore the influence of organic bridging ligands on the complex architectures, three related flexible bis(imidazole) ligands bix, bmimb, and bimb were employed. As to **1**, **2**, and **4**, all the reaction conditions are the same except for ancillary flexible bis(imidazole) ligands. As a result, complex **1** is a 3-D five-fold interpenetration utp topology

network containing left- and right-hand 2_1 helical CuCN chains. While in **2**, generated from a pendant substituent ligand bmimb than that in **1**, a different 3-D three-fold interpenetration $ThSi_2$ topology network containing *meso* helical CuCN chains was generated. However, in **4**, obtained from long ligand bimb, its network is simple distorted 2-D (6,3) layer with zigzag CuCN chains. Moreover, complexes **2** and **3** exhibit the effect of the reaction solvents on the complex architectures. Complex **3** present a different 3-D three-fold interpenetration utq topology network containing left- and right-hand 2_1 helical CuCN chains. From the above points discussed, it is suggested that the resulting structure change may be attributed to the inherent flexible nature of CuCN chains.

3.5. Thermal gravimetric analyses

To verify the thermal stabilities of **1**–**4**, thermogravimetric analyses (TG) were carried out under an N_2 atmosphere with a heating rate of 10 °C min^{-1}. As shown in Fig. S5, complexes **1**–**4** show no weight loss until the temperature reaches 330, 300, 335 and 360 ºC, respectively, and after that temperature, they begin to decompose, and that they all do not decompose completely until 800 ºC. The rapid weight loss for **1**–**4** is observed, which is attributed to the decomposition of the flexible bis(imidazole) ligand and cyanide group. The results of the TG analysis indicate that **1–4** would have good thermal stabilities.

3.4. Photoluminescent properties

The emission spectra of **1**–**4** in the solid state at room temperature are presented in Fig. 5. The strong emission peak of **1** is observed at 553 nm (λ_{ex} = 290 nm). Complexes **2** and **3** have almost the same emission band with the emission peak at ~ 565 nm (λ_{ex} = 300 nm). Complex **4** shows the emission band centered at 563 nm (λ_{ex} = 300 nm). In contrast to the luminescent properties of the reported complexes of copper(I) cyanide and heterocyclic ligands. The emission spectra should be generally

assigned as a metal-to-ligand charge transfer (MLCT) state or a ligand-to-ligand charge transfer (LLCT) state because of their structureless emission spectra.[21] To further obtain the luminescence and electronic properties of **1-4**, the DFT and TDDFT calculations were performed on the selected models (Fig. S6). Fig. S7 represents the distribution patterns of near-frontier molecular orbital of **1**-**4**, which play an underlying role in the electric structures and spectroscopic properties. It can be found that the highest occupied molecular orbitals (HOMOs) of **1**-**4** are basically localized on one cyanide anion and one copper(I) center while the near-lowest unoccupied molecular orbitals (LUMOs for **1**-**3** and LUMO+1 for **4**) are principally on other one cyanide anion. The complete spatial separation of these near-frontier orbitals exhibits that the HOMO→LUMO (**1**-**3**)/LUMO+1 (**4**) transition possesses significant charge transfer character. For **1**-**3**, The TDDFT computations indicate the $S_0 \rightarrow S_1$ vertical electronic transition can be dominated by the HOMO→LUMO contribution (100% (**1**), 98% (**2** and **3**)), showing a marginal oscillator strength f = 0.0146, 0.0007 and 0.0005, respectively. In prominent contrast, the $S_0 \rightarrow S_1$ electronic excitation of **4** is not an allowed electric-dipole transition (f = 0.0000). The allowed lower $S_0 \rightarrow S_2$ electronic excitation is dominated by the HOMO→LUMO+1 contribution (98%) with f = 0.0227. So the intense green experimental band of complex **1**-**4** may be assigned to a combination of the metal-to-ligand(CN) charge transfer (MLCT) and ligand(CN)-to-ligand(CN) charge transfer (LLCT) transitions.

4. Conclusions

In conclusion, Four new CuCN complexes containing auxiliary flexible bis(imidazole) ligands have been prepared *via* a simultaneous redox and self-assembly reaction of copper(II) used as starting materials under solvothermal conditions. These complexes present fascinating 2-D and 3-D networks with interesting topologies. The structural diversities of the CuCN complexes indicate the nature of auxiliary flexible bis(imidazole) ligands and solvents plays a substantial role in the formation of the novel coordination architectures, and the successful syntheses of the four new

complexes show that it is promising to obtain intriguing structures and properties *via* modifying the auxiliary ligands or solvents. Moreover, complexes **1**-**4** promise substitutions of the noble metals for the green luminescent materials due to their high thermal stability and strong green emission.

Acknowledgments

This work was supported by the NSFC (No. 21407004) and the Outstanding Youth Foundation of the Education Commission of Anhui Province, China (No. 2010SQRL108ZD).

Appendix A. Supplementary material

CCDC 979081-979084 contain the supplementary crystallographic data for **1-4**. These data can be obtained from the Cambridge Crystallographic Data Centre via http://www.ccdc.cam.ac.uk/conts/retrieving.html. Supplementary data associated with this article can be found, in the online version, at http://dx.doi.

References

1 (a) B. Zheng, H. Dong, J. F. Bai, Y. Z. Li, S. H. Li and M. Scheer, *J. Am. Chem. Soc*., 2008, **130**, 7778; (b) L. Brammer, *Chem. Soc. Rev*., 2004, **33**, 476. (c) M. D. Allendorf, C. A. Bauer, R. K. Bhakta and R. J. T. Houk, *Chem. Soc. Rev*., 2009, **38**, 133; (d) O. M. Yaghi, M. O'Keeffe, N. W. Ockwig, H. K. Chae, M. Eddaoudi and J. Kim, *Nature*, 2003, **423**, 705.

2 (*a*) H. Furukawa, N. Ko, Y. B. Go, N. Aratani, S. B. Choi, E. Choi, A. Ö. Yazaydin, R. Q. Snurr, M. O'Keeffe, J. Kim and O. M. Yaghi, *Science*, 2010, **329**, 424; (*b*) D. Tanaka, A. Henke, K. Albrecht, M. Moeller, K. Nakagawa, S. Kitagawa and J. Groll, *Nat. Chem*., 2010, **2**, 410; (*c*) D. Liu, Z. G. Ren, H. X. Li, J. P. Lang, N. Y. Li and B. F. Abrahams, *Angew. Chem., Int. Ed*., 2010, **49**, 4767. (*d*) X. L.Wang, C. Qin, S. X. Wu, K. Z. Shao, Y. Q. Lan, S. Wang, D. X. Zhu, Z. M. Su and E. B. Wang, *Angew. Chem., Int. Ed*., 2009, **48**, 5291; (*e*) P. N. Trikalitis,

K. K. Rangan, T. Bakas and M. G. Kanatzidis, *J. Am. Chem. Soc*., 2002, **124**, 12255; (*f*) M. V. Vasylyev and R. Neumann, *J. Am. Chem. Soc*., 2004, **126**, 884; (g) S. C. Xiang, X. T. Wu, J. J. Zhang, R. B. Fu, S. M. Hu and X. D. Zhang, *J. Am. Chem. Soc*., 2005, **127**, 16352; (*h*) B. Chen, L. Wang, F. Zapata, G. Qian and E. B. Lobkovsky, *J. Am. Chem. Soc*., 2008, **130**, 6718; (*i*) M. Sadakiyo, T. Yamada and H. Kitagawa, *J. Am. Chem. Soc*., 2009, **131**, 9906; (*j*) L. J. Murray, M. Dincâ and J. R. Long, *Chem. Soc. Rev*., 2009, **38**, 1294; (*k*) W. Walker, S. Grugeon, O. Mentre, S. Laruelle, J. M. Tarascon and F. Wudl, *J. Am. Chem. Soc*., 2010, **132**, 6517. (*l*) B. S. Zheng, J. F. Bai, J. G. Duan, L.Wojtas and M. J. Zaworotko, *J. Am. Chem. Soc*., 2011, **133**, 748; (*m*) M. D. Allendorf, C. A. Bauer, R. K. Bhakta and R. J. T. Houk, *Chem. Soc. Rev*., 2009, **38**, 1330; (*n*) J. Yang, B. Li, J. F. Ma, Y. Y. Liu and J. P. Zhang, *Chem. Commun*., 2010, **46**, 8383; (o) T. Y. Shvareva, S. Skanthakumar, L. Soderholm, A. Clearfield and T. E. Albrecht-Schmitt, *Chem. Mater*., 2007, **19**, 132.

3 (*a*) R.C. Evans, P. Douglas, and C. J. Winscom, *Coord. Chem. Rev*., 2006, **250**, 2093; (*b*) Y. Chi, and P. T. Chou, *Chem. Soc. Rev*., 2010, **39**, 638; (*c*) Q. Zhao, F. Li, and C. Huang, *Chem. Soc. Rev*., 2010, **39**, 3007; (*d*) Y. You, and W. Nam, *Chem. Soc. Rev*., 2012, **41**, 7061; (*e*) H. Sun, L. Yang, H. Yang, S. Liu, W. Xu, X. Liu, Z. Tu, H. Su, Q. Zhao, and W. Huang, *RSC Adv*., 2013, **3**, 8766; (*f*) J. Liu, Y. Liu, Q. Liu, C. Li, L. Sun, and F. Li, *J. Am. Chem. Soc*., 2011, **133**,15276.

4 H. Yersin, *Highly Efficient OLEDs with Phosphorescent Materials*; Wiley-VCH Verlag GmbH & Co. KGaA: Weinheim, Germany, 2008

5 (*a*) N. Greenwood, and A. Earnshaw, *Chemistry of the Elements, 2nded.*; Elsevier: Oxford, U.K., 1997. (*b*) M. Wallesh, D. Volz, D.M. Zink, U. Schepers, M. Nieger, T. Baumann, and S. Bräse, *Chem. ・ Eur. J*., 2014, **20**, 6578; (*c*) D. Volz, M. Nieger, J. Friedrichs, T. Baumann, and S. Bräse, *Langmuir*, 2013, **29**, 3034; (*d*) M. J. Leitl, F. R. Küchle, H. A. Mayer, L. Wesemann, and H. Yersin, *J. Phys. Chem. A*, 2013, **117**, 11823; (*e*) X. L. Xin, M. Chen, Y. B. Ai, F. L. Yang, X. L. Li, and F. Y. Li, *Inorg. Chem.*, 2014, 53, 2922; (*f*) R. Marion, F. Sguerra, F. D. Meo, E.

Sauvageot, J. F. Lohier, R. Daniellou, J. L. Renaud, M. Linares, M. Hamel, and S. Gaillard, *Inorg. Chem*., 2014, **53**, 9181.

6 (*a*) A. J. Blake, N. R. Brooks, N. R. Champness, M. Crew, A. Deveson, D. Fenske, D. H. Gregory, L. R. Hanton, P. Hubberstey and M. Schröder, *Chem. Commun*., 2001, 1432; (*b*) Y. J. Qi, Y. H. Wang, C. W. Hu, M. H. Cao, L. Mao and E. B. Wang, *Inorg. Chem*., 2003, **42**, 8519. (*c*) V. S. S. Kumar, F. C. Pigge and N. P. Rath, *New J. Chem*., 2004, **28**, 1192; (*d*) B. Li, G. Li, D. Liu, Y. Peng, X. Zhou, J. Hua, Z. Shi and S. Peng, *CrystEngComm*, 2011, **13**, 1291.

7 (a) A. P. Cote, A. I. Benin, N. W. Ockwig, M. O'Keeffe, A. J. Matzger and O. M. Yaghi, *Science*, 2005, **310**, 1166; (b) X. Y. Wang, L. Wang, Z. M. Wang and S. Gao, *J. Am. Chem. Soc*., 2006, **128**, 674; (c) S. Hasegawa, S, Horike, R. Matsuda, S. Furukawa, K. Mochiźuki, Y. Kinoshita and S. Kitagawa, *J. Am. Chem. Soc*., 2007, **129**, 2607; (d) R. Vilar, *Angew. Chem. Int. Ed*., 2003, **42**, 1460; (e) P. X. Yin, J. Zhang, Y. Y. Qin, J. K. Cheng, Z. J. Li and Y. G. Yao, *CrystEngComm*, 2011, **13**, 3536; (f) J. Q. Liu, Y. Y. Wang and Y. S. Huang, *CrystEngComm*, 2011, **13**, 3733; (g) Y. B. Zhang, W. X. Wang, F. Y. Feng, J. P. Zhang and X. M. Chen, *Angew. Chem. Int. Ed*., 2009, **48**, 5287.

8 (*a*) J. Xu, Z. R. Pan, T. W. Wang, Y. Z. Li, Z. J. Guo, S. R. Batten and H. G. Zheng, *CrystEngComm*, 2010, **12**, 612; (*b*) J. Y. Lu, *Coord. Chem. Rev*., 2003, **246**, 327; (*c*) Y. Xu, P. K. Chen, Y. X. Che and J. M. Zheng, *Eur. J. Inorg. Chem*., 2010, 5478; (*d*) J. R. Li, D. J. Timmons and H. C. Zhou, *J. Am. Chem. Soc*., 2009, **131**, 6368; (*e*) J. C. Jin, Y. N. Zhang, Y. Y. Wang, J. Q. Liu, Z. Dong and Q. Z. Shi, *Chem.-Asian J*., 2010, **5**, 1611; (*f*) E. C. Yang, Z. Y. Liu, X. J. Shi, Q. Q. Liang and X. J. Zhao, *Inorg. Chem*., 2010, **49**, 7969

9 (*a*) Q. Chu, G. X. Liu, Y. Q. Huang, X. F. Wang and W. Y. Sun, *Dalton Trans*., 2007, 4302; (*b*) Y. Qi, Y. X. Che and J. M. Zheng, *Cryst. Growth Des.*, 2008, **8**, 3602; (*c*) G. H. Wei, Y. Yang, J. F. Ma, Y. Y. Liu, S. L. Li and L. P. Zhang, *Dalton Trans*., 2008, 3080; (*d*) L. L. Wen, F, Wang, J. Feng, K. L. Lv, C. G. Wang and D. F. Li, *Cryst. Growth Des.*, 2009, **9**, 3581; (*e*) S, Zhang, S. Yang, J. Lan, Y. Tang, Y. Xue and J. You, *J. Am. Chem. Soc*., 2009, **131**, 1689; (*f*) G. S. Yang, Y. Q. Lan, H.

Y. Zang, K. Z. Shao, X. L. Wang, Z. M. Su and C. J. Jiang, *CrystEngComm*, 2009, **11**, 274; (g) Z. X. Li, X. Chu, G. H. Cui, Y. Liu, L. Li and G. L. Xue, *CrystEngComm*, 2011, **13**, 1984.

10 (*a*) G. X. Liu, K. Zhu, H. M. Xu, S. Nishihara, R. Y. Huang and X. M. Ren, *CrystEngComm*, 2010, **12**, 1175; (*b*) G. X. Liu, R. Y. Huang, L. F. Huang, X. J. Kong and X. M. Ren, *CrystEngComm*, 2009, **11**, 643; (*c*) G. X. Liu, K. Zhu, H. M. Xu, S. Nishihara, R. Y. Huang and X. M. Ren, *CrystEngComm*, 2009, **11**, 2784; (*d*) G. X. Liu, K. Zhu, H. Chen, R. Y. Huang, H. Xu and X. M. Ren, *Inorg. Chim. Acta*, 2009, **362**, 1605; (*e*) G. X. Liu, K. Zhu, S. Nishihara, R. Y. Huang and X. M. Ren, *Inorg. Chim. Acta*, 2009, **362**, 5103; (*f*) G. X. Liu, R. Y. Huang, H. Xu, X. J. Kong, L. F. Huang, K. Zhu and X. M. Ren, *Polyhedron*, 2008, **27**, 2327; (*g*) G. X. Liu, K. Zhu, H. Chen, R. Y. Huang and X. M. Ren, *CrystEngComm*, 2008, **10**, 1527; (*h*) R. Y. Huang, H. Xu, S. Y. Ye, G. H. Wu, X. Q. Zhao, Y. Wang and G. X. Liu, *J. Mol. Struct.,* 2013, **1036**: 235.

11 H. K. Liu, W. Y. Sun, H. L. Zhu, K. B. Yu, and W. X. Tang, *Inorg Chem Acta*, 1999, **295**, 129.

12 (*a*) G. M. Sheldrick, *SHELXS-97, Program for Crystal Structure Solution*, University of Göttingen, Germany, 1997; (*b*) G. M. Sheldrick, *SHELXL-97, Program for Crystal Structure Refinement*, University of Göttingen, Germany, 1997.

13 M. J. Frisch, G. W. Trucks, H. B. Schlegel, G. E. Scuseria, M. A. Robb, J. R. Cheeseman, G. Scalmani, V. Barone, B. Mennucci, G. A. Petersson, H. Nakatsuji, M. Caricato, X. Li, H. P. Hratchian, A. F. Izmaylov, J. Bloino, G. Zheng, J. L. Sonnenberg, M. Hada, M. Ehara, K. Toyota, R. Fukuda, J. Hasegawa, M. Ishida, T. Nakajima, Y. Honda, O. Kitao, H. Nakai, T. Vreven, J. A. Montgomery Jr., J. E. Peralta, F. Ogliaro, M. Bearpark, J. J. Heyd, E. Brothers, K. N. Kudin, V. N. Staroverov, R. Kobayashi, J. Normand, K. Raghavachari, A. Rendell, J.C. Burant, S. S. Iyengar, J. Tomasi, M. Cossi, N. Rega, J. M. Millam, M. Klene, J. E. Knox, J. B. Cross, V. Bakken, C. Adamo, J. Jaramillo, R. Gomperts, R. E. Stratmann, O. Yazyev, A. J. Austin, R. Cammi, C. Pomelli, J. W. Ochterski, R. L. Martin, K.

Morokuma, V. G. Zakrzewski, G. A. Voth, P. Salvador, J. J. Dannenberg, S. Dapprich, A. D. Daniels, O. Farkas, J. B. Foresman, J. V. Ortiz, J. Cioslowski, and D. J. Fox, Gaussian 09, Revision D.01, Gaussian, Inc., Wallingford, CT, 2013.

14 (*a*) A. D. Becke, Phys. Rev. A, 1998, **38**, 3098; (*b*) C. Lee, W. Yang, and R. G. Parr, Phys. Rev. B, 1988, **37**, 785.

15 M. J. Frisch, J. A. Pople, and J. S. Binkley, *J. Chem. Phys*., 1984, **80**, 3265.

16 (*a*) P. J. Hay, and W. R. Wadt, *J. Chem. Phys*., 1985, **82**, 270; (*b*) P. J. Hay, and W. R. Wadt, *J. Chem. Phys*., 1985, **82**, 299.

17 (*a*) O. M. Yaghi, and H. Li, *J. Am. Chem. Soc.*, 1995, **117**, 10401; (b) Z. F. Zhao, B. B. Zhou, Z. H. Su, H. Y. Ma and C. X. Li, *Inorg. Chem. Commun*., 2008, **11**, 648; (*c*) Z. H. Su, Z. F. Zhao, B. B. Zhou, Q. H. Cai and Y. Zhang, *CrystEngComm*, 2011, **13**, 1474.

18 V. A. Blatov, A. P. Shevchenko and D. M. Proserpio, *Cryst. Growth Des*., 2014, **14**, 3576.

19 A. F. Wells, *Three-dimensional nets and polyhedral*, *Wiley-Interscience*: *New York*, 1977.

20 V. A. Blatov, L. Carlucci, G. Ciani and D. M. Proserpio, *CrystEngComm*, 2004, **6**, 377.

21 (*a*) J. P. Zhang, Y. Y. Lin, X. C. Huang and X. M. Chen, *J. Am. Chem. Soc*., 2005, **127**,5495; (*b*) H. Araki, K. Tsugge, Y. Sasaki, S. Ishizaka and N. Kitamura, *Inorg. Chem.* 2005, **44**, 9667; (*c*) D. Li W. J. Shi and L. Hou, *Inorg. Chem*. 2005, **44**, 3907; (*d*) P. C. Ford, E. Cariati and J. Bourassa, Chem. Rev. 1999, **99**, 3625.

22

Captions for Figures

Figure 1. (a) Coordination environment of the Cu(I) atom in **1** with the ellipsoids drawn at the 30% probability level, all hydrogen atoms were omitted for clarity. (b) A perspective view of the left- and right-hand 2_1-helical CuCN chains in **1**. (c) The 3-D (10, 3)-d network in **1**. (d) Schematic representations of five-fold interpenetrating (10, 3)-d network in **1**. (e) The self-penetrated binodal (3,6)-connected network in **1**. (red balls, Cu2 atoms; blue balls, $(Cu1)_2$ dimers; magenta line, 6-membered circuit; green line, 10-membered circuit).

Figure 2. (a) Coordination environment of the Cu(I) atom in 2 with the ellipsoids drawn at the 30% probability level, all hydrogen atoms are omitted for clarity. (b) 1D *meso*-helical CuCN chain structure along the [101] direction in **2**. (c) The 3-D (10, 3)-b network in **2**. (d) Schematic representations of three-fold interpenetrating (10, 3)-b network in **2**.

Figure 3. (a) Coordination environment of the Cu(I) atom in **3** with the ellipsoids drawn at the 30% probability level, all hydrogen atoms are omitted for clarity. (b) A perspective view of the left- and right-hand 2_1-helical CuCN chains in **3**. (c) Overview of 3-D $3/10/t_2$ network in **3**. (d) Schematic representations of three-fold interpenetrating utq network in **3**.

Figure 4. (a) Coordination environment of the Cu(I) atom in **4** with the ellipsoids drawn at the 30% probability level, all hydrogen atoms are omitted for clarity. (b) 1-D zigzag CuCN chain structure in **4**. (c) A perspective view of the 2-D (6, 3) layer in **4**. (d) Schematic representations of the 3-D supramolecular stacking structure in **4**.

Figure 5. Solid-state emission spectra of **1**-**4** at ambient temperature.

Table 1

Crystallographic data and structure refinement summary for **1-4**

Complexes	**1**	**2**	**3**	**4**
Empirical formula	$C_{16}H_{14}N_6Cu_2$	$C_9H_9N_3Cu$	$C_9H_9N_3Cu$	$C_{23}H_{18}N_7Cu_3$
Formula weight	417.41	222.73	222.73	583.06
Crystal system	Monoclinic	Monoclinic	Orthorhombic	Triclinic
Space group	$P2_1/c$	$C2/c$	$Fddd$	P-1
a / Å	8.7916(4)	15.7226(6)	13.868(3)	7.3383(9)
b / Å	15.3787(7)	14.1888(6)	22.973(4)	9.7110(11)
c / Å	14.4000(5)	9.1539(3)	24.215(4)	9.8336(12)
α / °	90	90	90	61.160(7)
β / °	122.692(2)	101.662(3)	90	73.893(9)
γ / °	90	90	90	74.296(8)
V / Å^3	1638.51(12)	1999.94(13)	7715(2)	581.90(12)
Z	4	8	32	1
T / K	293(2)	296(2)	296(2)	296(2)
D_{cacl} (g·cm^{-3})	1.692	1.479	1.534	1.664
μ / mm^{-1}	2.605	2.139	2.218	2.742
F(000)	840	904	3616	292
Data collected	12449	13215	6519	6695
Independent data	2906	1775	1689	2025
R_{int}	0.0275	0.1398	0.0698	0.2500
Data/restraints/parameters	2906 / 1 / 217	1775 / 0 / 121	1689 / 0 / 119	2025 / 0 / 151
Goodness-of-fit	1.006	1.002	1.004	1.009
R_1 $[I > 2\sigma(I)]^a$	0.0259	0.0334	0.0387	0.0678
wR_2 $[I > 2\sigma(I)]^b$	0.0662	0.0993	0.1046	0.1921

^{a} $R_1 = \Sigma||F_o| - |F_c||/\Sigma|F_o|$. ^{b} $wR_2 = |\Sigma w(|F_o|^2 - |F_c|^2)|/\Sigma|w(F_o)^2|^{1/2}$, $w = 1/[\sigma^2(F_o^2) + (aP)^2 + bP]$. $P = (F_o^2 + 2F_c^2)/3$.

Table 2

Selected bond lengths (Å) and angles (°) for **1-4**

$Cu_4(CN)_4(bix)_2$ (1)			
Cu(1)–C(1)	1.917(3)	C(1)–Cu(1)–N(2)	121.31(10)
Cu(1)–N(2)	2.001(2)	C(1)–Cu(1)–N(3)	123.47(10)
Cu(1)–N(3)	2.040(2)	N(2)–Cu(1)–N(3)	99.04(8)
Cu(2)–C(2)	1.879(2)	C(2)–Cu(2)–N(1)#1	143.72(10)
Cu(2)–N(1)#1	1.912(2)	C(2)–Cu(2)–N(5)	112.21(9)
Cu(2)–N(5)	2.057(2)	N(1)#1–Cu(2)–N(5)	104.03(8)
$Cu_2(CN)_2$(bmimb) (2)			
Cu(1)–X(2)	1.871(2)	X(2)–Cu(1)–X(1)	129.30(11)
Cu(1)–X(1)	1.894(2)	X(2)–Cu(1)–N(3)	120.92(9)
Cu(1)–N(3)	2.0148(17)	X(1)–Cu(1)–N(3)	109.16(9)
$Cu_2(CN)_2$(bmimb) (3)			
Cu(1)–X(1)	1.905(3)	X(2)–Cu(1)–X(1)	123.60(13)
Cu(1)–X(2)	1.887(3)	X(2)–Cu(1)–N(3)	123.50(13)
Cu(1)–N(3)	1.987(3)	X(1)–Cu(1)–N(3)	112.41(13)
$Cu_3(CN)_3$(bimb) (4)			
Cu(1)–C(2)	1.867(7)	C(2)–Cu(1)–X(1)	134.7(2)
Cu(1)–X(1)	1.930(5)	C(2)–Cu(1)–N(3)	120.7(2)
Cu(1)–N(3)	2.012(5)	X(1)–Cu(1)–N(3)	103.8(2)
Cu(2)–N(2)	1.841(8)	N(2)–Cu(2)–N(2)#2	180.00

Symmetry transformations used to generate equivalent atoms: #1 –x + 3, y – 1/2, –z + 3/2; #2 –x + 3, –y + 1, –z + 2

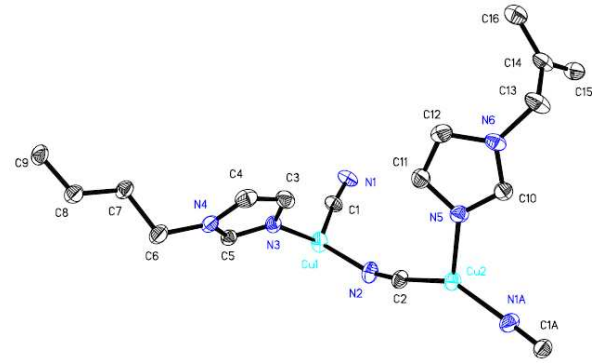

(a)

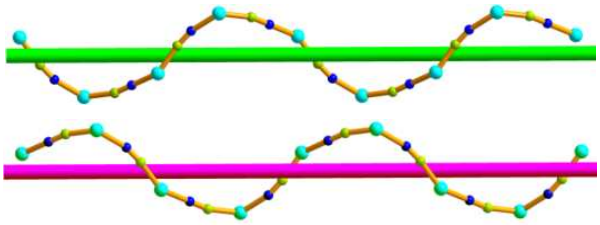

(b)

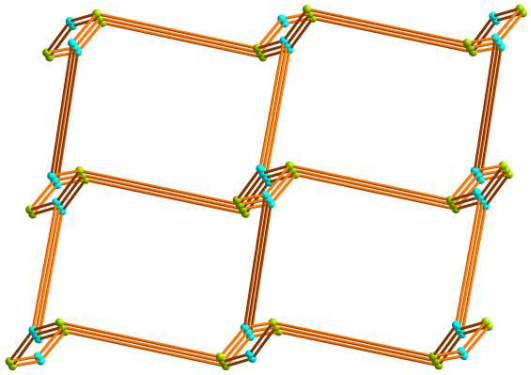

(c)

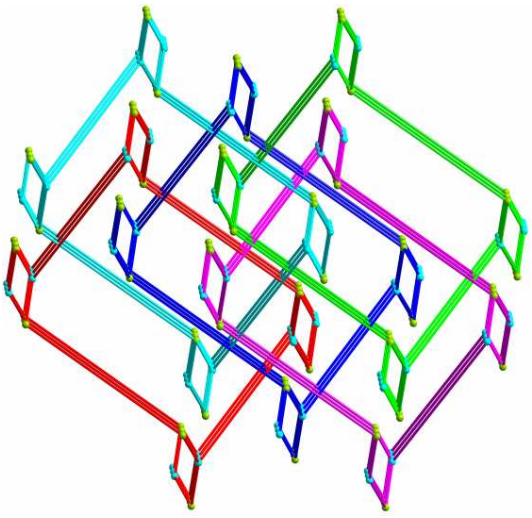

(d)

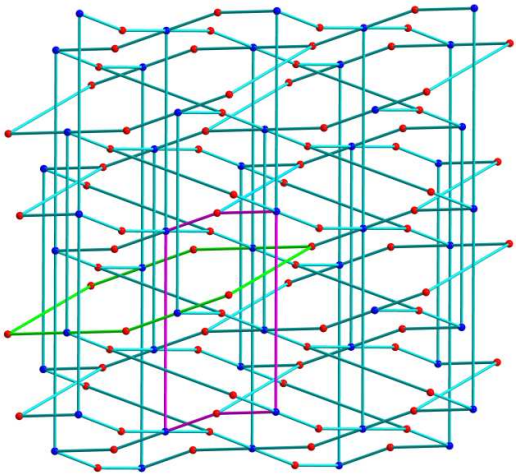

(e)

Figure 1.

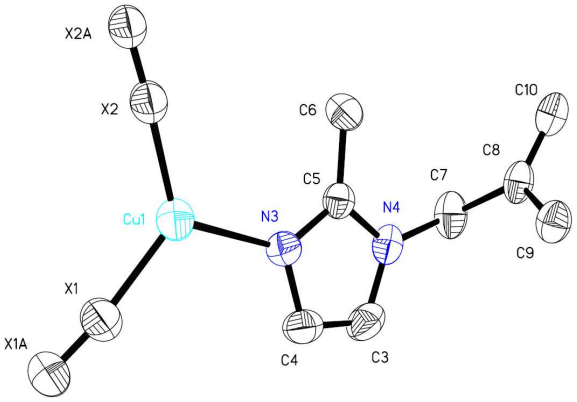

(a)

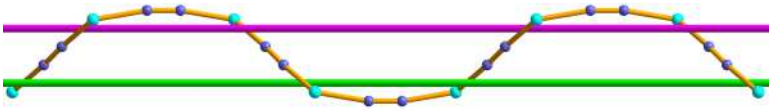

(b)

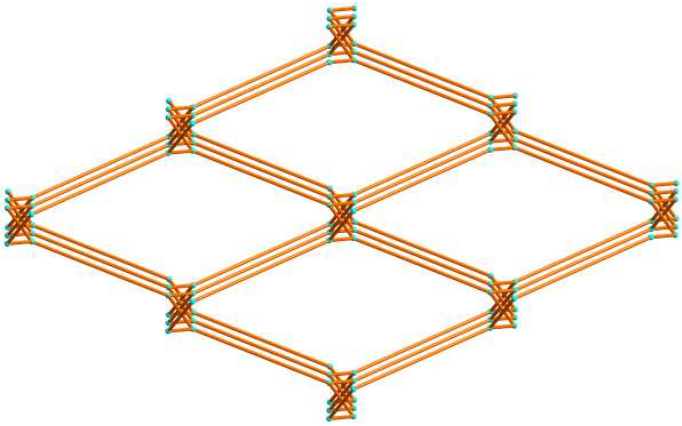

(c)

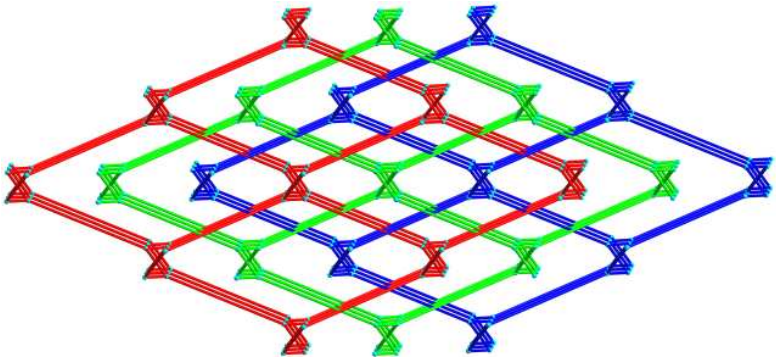

(d)

Figure 2.

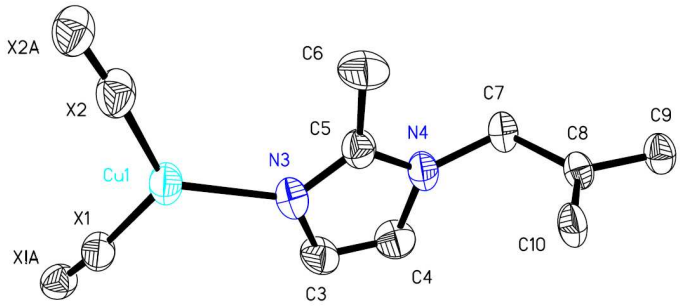

(a)

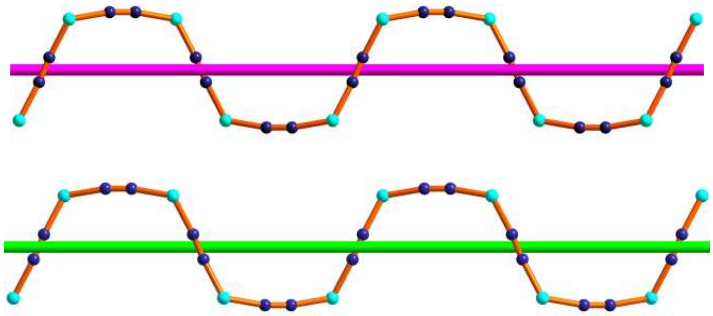

(b)

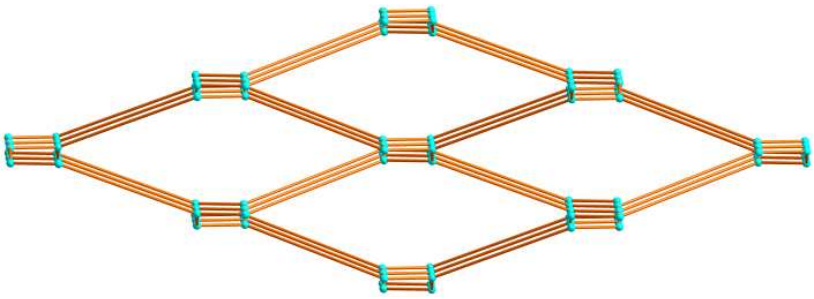

(c)

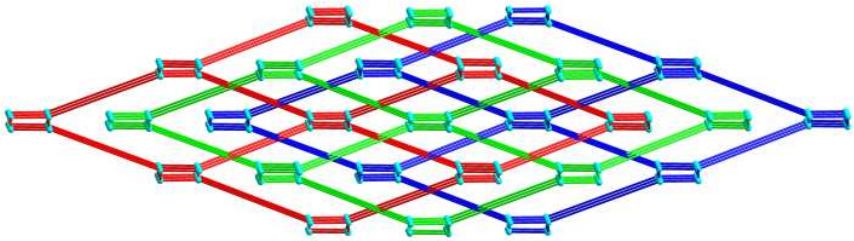

(d)

Figure 3.

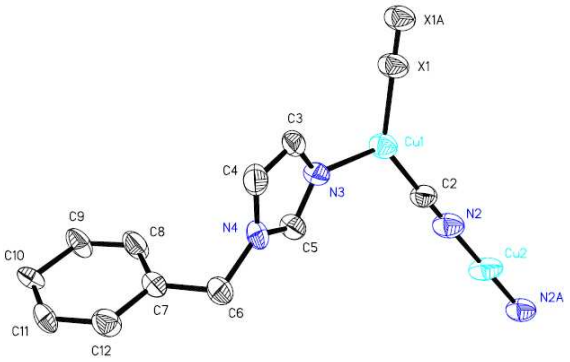

(a)

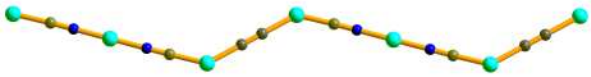

(b)

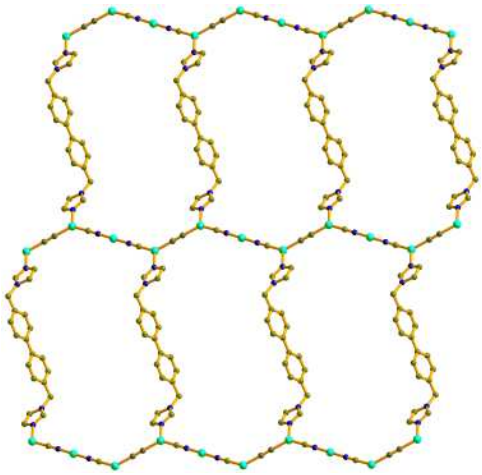

(c)

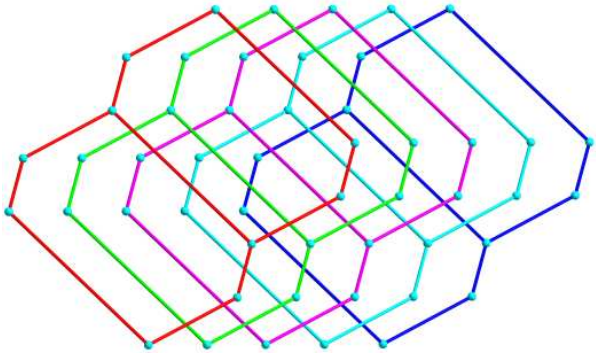

(d)

Figure 4.

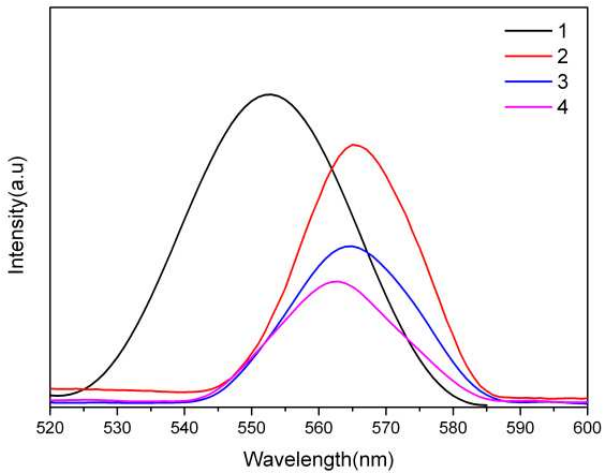

Figure 5.